magnetochemistry

MDPI

Article

Size and Ion-Doping Effects on Magnetic, Optical, and Phonon Properties of $CuAlO_2$ Nanoparticles

Iliana Naumova Apostolova [1], Angel Todorov Apostolov [2] and Julia Mihailova Wesselinowa [3,*]

[1] Faculty of Forest Industry, University of Forestry, 1756 Sofia, Bulgaria
[2] Faculty of Hydrotechnics, University of Architecture, Civil Engineering and Geodesy, 1046 Sofia, Bulgaria
[3] Department of Physics, University of Sofia, 1164 Sofia, Bulgaria
* Correspondence: julia@phys.uni-sofia.bg

Abstract: The magnetic, optical, and phonon properties of ion-doped $CuAlO_2$ nanoparticles on the Cu or Al site are theoretically investigated. The room temperature ferromagnetism in $CuAlO_2$ nanoparticles can be due to the surface, size, and doping effects. The magnetization increases with the decreasing nanoparticle size. The different radii of the transition metal ion and the host Cu ion lead to compressive strain, to the enhancment of the exchange interaction constants, and to increased magnetization M_s and Curie temperature T_C. By substitution with Mn or Cr on the Al site, tensile strain, a decrease in M_s, and an increase in dopants are observed. The size and ion-doping influence on the band-gap energy is also discussed. The phonon energy ω decreases, whereas the phonon damping γ increases with increasing temperature and decreasing NP size. They show a kink around $T_C \sim 400$ K. The behavior of ω and γ for different ion dopings is observed.

Keywords: $CuAlO_2$; ion doping; magnetization; band gap; phonon energy; microscopic model

Citation: Apostolova, I.N.; Apostolov, A.T.; Wesselinowa, J.M. Size and Ion-Doping Effects on Magnetic, Optical, and Phonon Properties of $CuAlO_2$ Nanoparticles. *Magnetochemistry* **2022**, *8*, 169. https://doi.org/10.3390/magnetochemistry8120169

Academic Editors: Cătălin-Daniel Constantinescu and Lucian Petrescu

Received: 17 October 2022
Accepted: 22 November 2022
Published: 25 November 2022

1. Introduction

Diluted magnetic semiconductors (DMS) play an important role in interdisciplinary materials science and future spintronics. Ferromagnetic DMS have been studied from first principles within mean field approximation [1,2]. Ferromagnetism in 3d transition metal (TM)-doped II–VI and III–V based DMS is predicted [3]. Kizaki et al. [4] have investigated the magnetism in a new DMS, namely $CuAlO_2$ (CAO), by the Korringa–Kohn–Rostoker method. Using density functional theory (DFT) calculations, Iordanidou et al. [5] have examined the hole doping effect on the magnetic and electronic properties of CAO. It is known that pure CAO is a p-type width band gap semiconductor with E_g of about 3.5 eV [6]. It has the hexagonal delafossite structure and the space group of $R\bar{3}m$. CAO can be applied as a DMS when doped with TM ions. Kizaki et al. [4,7] have investigated the electronic and magnetic properties under carrier doping treatment in TM-doped CAO on the Cu site (TM = Fe, Co, Mn, and Ni). The Curie temperature T_C of the doped examples increases with increasing dopant concentration. Moreover, Fe or Co doping on the Al site of CAO bulk and thin films increases the spontaneous magnetization [8–12].

The origin of ferromagnetism in DMS is not yet clear, even if various methods have been proposed. First-principal calculations showed that $(Cu,Fe)AlO_2$ can be a candidate of ferromagnetic DMS [13]. From the calculated density of states, it seems that the double exchange interaction is the dominant exchange mechanism in $(Cu,Fe)AlO_2$ [13]. It was recently found that the weak magnetism of these materials may derive from the polarised unpaired electrons around impurities [14]. The magnetic properties of Mn-doped CAO, $Cu(Al,Mn)O_2$ have been reported by Zhang et al. [15]. The magnetization decreases with increasing Mn concentration. The influence of Cd impurity at Cu and Al sites on the electronic properties of CAO from first-principles calculations is discussed in Ref. [16].

The TM doping on the Al site also influences the optical properties of CAO thin films and nanofibers [17–21]. Raman spectra of pure and ion-doped CAO bulk and NPs are

studied in [18,22–26]. So, carrier concentration and ion doping together significantly affect the oxide-based DMS.

The aim of the present paper is to investigate the magnetic, optical, and phonon properties of ion-doped CAO nanoparticles (NPs) for the first time using a microscopic model and Greens's function theory in order to clarify the origin of room temperature ferromagnetism in these systems on microscopic level.

It should be noted that the most theoretical papers consider the magnetic properties of CAO NPs using DFT. The DFT is a very powerful tool in investigation of many body problems. However, DFT is mostly concerned with ground-state properties at zero temperature. In our approach, we are able to cover the whole temperature regime. It is a finite temperature analysis including the entire excitation spectrum. In particular, the method allows us to study the total phase diagram, which is based on the different excitation energies realized in the system. The disadvantage of our approach consists of the consideration of collective properties from the beginning. Our basic quantities are not the "naked" electrons but effective spins of the underlying quasi-particles. Whereas within DFT all of the parameters of the system can be—at least in principle—calculated, we are forced to use additional models to find out those parameters. We are convinced that both approaches, DFT and Green's function method, are appropriate and, to a certain extent, are an alternative in describing many body systems.

2. The Model and Green's Functions

The room temperature ferromagnetism in bulk CAO can be caused by ion doping and can be described by the Heisenberg hamiltonian H_d:

$$H_d = \sum_{i,j} x J_{dij}(\mathbf{S}_j \cdot \mathbf{S}_j) - \sum_i D_i (S_i^z)^2 - g\mu_B h \sum_i S_i^z. \quad (1)$$

$\mathbf{S}_i$ is the Heisenberg spin-operator of the TM at site i. J_d is the exchange interaction between the TM ions. Kizaki et al. [4] found that J_d between the magnetic ions in the same Cu-plane are ferromagnetic, whereas those between the Cu-planes can be neglected. D is the single-ion anisotropy, h is an external magnetic field, and x is the doping concentration.

In the case of a CAO NP, there also appears a ferromagnetism from surface and size effects due to the uncompensated Al spins on the surface described by H_s as well as due to ion-doping effects (see H_d):

$$H_s = -\sum_{i,j} (1-x) J_{sij}(\mathbf{S}_j \cdot \mathbf{S}_j). \quad (2)$$

From the spin Green's function defined as $G_{ij} = \ll S_i^+; S_j^- \gg$ the magnetization M for arbitrary spin S is calculated:

$$M = \frac{1}{N^2} \sum_k \Big[(S+0.5) \coth[(S+0.5)\beta E_m(\mathbf{k})] - 0.5 \coth(0.5\beta E_m(\mathbf{k}) \Big], \quad (3)$$

where $\beta = 1/k_B T$, $E_m(\mathbf{k})$ is the spin-wave energy.

The spin–phonon and phonon–phonon interactions are described by:

$$H_{sp-ph} = \frac{1}{2} \sum_{i,j,k} F(i,j,k) Q_i S_j^z S_k^z - \frac{1}{4} \sum_{i,j,r,s} R(i,j,r,s) Q_i Q_j S_r^z S_s^z + h.c. \quad (4)$$

The normal coordinate Q_i can be expressed in terms of phonon creation a^+ and annihilation a operators, $Q_i = (2\omega_{0i})^{-1/2}(a_i + a_i^+)$. F and R are the spin–phonon coupling constants in the first and second order, respectively.

$$\begin{aligned} H_{ph-ph} &= \frac{1}{2!}\sum_i \omega_{0i} a_i a_i^+ + \frac{1}{3!}\sum_{i,j,r} B(i,j,r) Q_i Q_j Q_r \\ &+ \frac{1}{4!}\sum_{i,j,r,s} A(i,j,r,s) Q_i Q_j Q_r Q_s, \end{aligned} \tag{5}$$

where ω_{0i} is the frequency of the lattice mode.

From the poles of the phonon Green's function $\tilde{G}_{ij}(t) = \langle\langle a_i(t); a_j^+ \rangle\rangle$ the phonon energies are observed:

$$\begin{aligned} \omega_{ij}^2 &= \omega_0^2 - 2\omega_0 \Big(M_i M_j R_{ij} \delta_{ij} \\ &- \frac{1}{2N'}\sum_r A_{ijr}(2\bar{N}_r + 1) - B_{ij}\langle Q_{ij}\rangle \delta_{ij} \Big), \end{aligned} \tag{6}$$

$$\langle Q_{ij}\rangle = \frac{M_i M_j F_{ij}\delta_{ij} - \frac{1}{N'}\sum_r B_{ijr}(2\bar{N}_r + 1)}{\omega_0 - M_i M_j R_{ij}\delta_{ij} + \frac{1}{N'}\sum_r A_{ijr}(2\bar{N}_r + 1)}. \tag{7}$$

The phonon correlation function $\bar{N}_r = \langle a_r^+ a_r \rangle$ is obtained via the spectral theorem. The phonon damping $\gamma = \gamma_{sp-ph} + \gamma_{ph-ph}$ is also calculated taking into account anharmonic spin–phonon and phonon–phonon interactions.

The band-gap energy E_g of a CAO NP is defined by the difference between the valence and conduction bands:

$$E_g = \omega^+(\mathbf{k} = 0) - \omega^-(\mathbf{k} = \mathbf{k}_\sigma). \tag{8}$$

The electronic energies

$$\omega^\pm(k) = \epsilon_k - \frac{\sigma}{2} I \langle S^z \rangle \tag{9}$$

are observed from the Green's function $g(k,\sigma) = \ll c_{k,\sigma}; c_{k\sigma}^+ \gg$, $\sigma = \pm 1$, $c_{i\sigma}^+$ and $c_{i\sigma}$ are Fermi operators, and I-s-d is the interaction constant [27].

3. Numerical Results and Discussion

A CAO NP with a cubo-octahedral shape is defined by fixing the origin at a certain Al spin in the center of the particle and including all other spins within the particle into shells, which are numbered by $n = 1, \ldots, N$ from the central to the surface shell. For the numerical calculations, we use the following model parameters: J_d(Fe-Fe) = 195 meV, J_d(Co-Co) = 117 meV, J_d(Mn-Mn) = 78 meV, J_d(Ni-Ni) = 97.5 meV [4], J_s = 20 meV, $D = -0.068$ meV, $F = 23$ cm^{-1}, $R = -18$ cm^{-1}, $A = 6.61$ cm^{-1}, and $B = -2.94$ cm^{-1}. The exchange interaction $J_{ij} = J(r_i - r_j)$ depends on the distance between the spins, i.e., on the lattice parameters. It is inverse proportional to the lattice parameters. Therefore, the exchange interaction constant on the surface J_s and of the doped states J_d can be changed or can increase or decrease in dependence on the strain in the lattice. So, we take into account the direct connection between the microstructure and magnetic behavior.

Firstly, we will consider the spontaneous magnetization M_s in a pure CAO NP. It must be noted that bulk CAO is a p-type wide band gap semiconductor, and it is a nonmagnetic compound. However, due to the uncompensated surface spins of the Al^{3+} ions on the surface, a spontaneous magnetization M_s appears in the CAO NP, contrary to the bulk case, where $M_s = 0$. We obtain that J_s increases and the spontaneous magnetization M_s of a CAO NP increases with decreasing NP size. The result is presented in Figure 1. A finite magnetization M_s is also observed experimentally in pure CAO NPs [12,28] and in pure CAO thin films [29], due to the existence of point defects. It must be noted that we obtain

similar behavior for the size dependence of the phase-transition temperature $T_C(N)$, T_C, which increases with decreasing NP size.

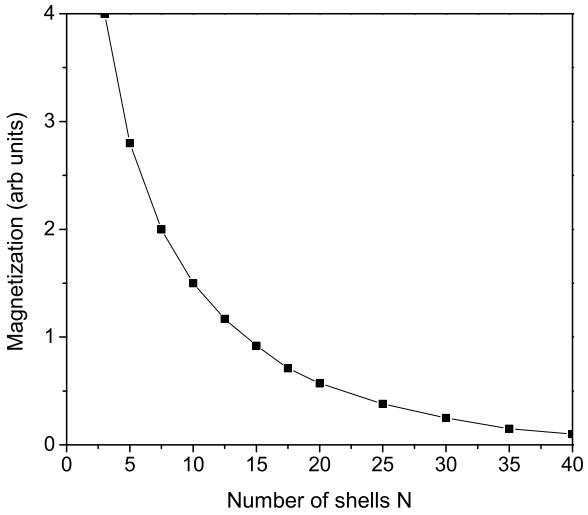

Figure 1. Size dependence of the spontaneous magnetization of a CAO NP for T = 300 K.

The origin of ferromagnetism in DMS is not yet clear. In order to investigate the observed room temperature ferromagnetism (RTFM) in ion-doped CAO-bulk and NPs, we have replaced some Cu-ions with Fe-ions, i.e., we consider $Cu_{1-x}Fe_xAlO_2$ NPs for x = 0–0.25. There are experimental data that show that in this concentration interval the samples are single-phase, whereas for larger x values, the second phase appears [4]. It must be noted that by the doping of TM on the Al site, the limit value of the ion doping concentration is smaller; it is around 0.05–0.1 [8,10,15,28,30], which is different for the different doping ions. The exchange interaction constant J depends on the distance between the spins, i.e., on the lattice parameter, on the different strain, on the lattice symmetry, and on the number of next neighbors. J is an inverse square function of the distance between two neighboring spins, i.e., $J \propto 1/(r_i - r_j)^2$. From the structural analysis, Cu^{1+} is replaced by Fe^{3+} or Fe^{2+}, which leads to cation vacancies increasing because of charge variation [4,7,9]. Through the different radii of the dopants, lattice defects can be introduced or intrinsic host-lattice defects can be activated when different ions, such as Fe, occupied the Cu sites. Chen et al. [9] have shown that Fe element exists in the ion form, with the valence of +2 and/or +3. Since the ionic radius of Fe^{2+} (0.92 $\dot{A}$) or Fe^{3+} (0.65 $\dot{A}$) is always smaller than Cu^{1+} (0.95 $\dot{A}$), the lattice parameters decrease with increasing the Fe dopants as supported by Chen et al. [9]. The reduction of the lattice constants in Fe-doped CAO nanostructures leads to a compressive strain, i.e., in our microscopic model, it leads to an increase in the exchange interaction constant of the doped states J_d with an increase in the Fe ion concentration because it is inverse proportional to the lattice parameters . So, we obtain an increase in the spontaneous magnetization M_s and the Curie temperature T_C. The ferromagnetic coupling between the doping Fe-ions contributes additively to this increase. Fe^{3+}-ion (Fe^{2+}-ion) has 5d (6d) electrons with the total spin of $S = 5/2$ ($S = 2$), whereas the Cu^{1+}-ion has $S = 0$. Thus, Fe^{3+} or Fe^{2+} substitution into Cu^{1+} induces an extra magnetic moment. The spontaneous magnetization M_s and the Curie temperature T_C in dependence on the Fe^{3+} doping concentration are calculated. We observe that both increase with increasing Fe doping concentration x. The result for $T_C(x)$ is demonstrated in Figure 2, curve 1. We would obtain a similar increase in the phase-transition temperature T_C, for example, for Ni-, Mn-, or Co-doped CAO, $(Cu,TM)AlO_2$ (Figure 2, curves 2–4), where the doping ions have a smaller ionic radius in comparison with that of the Cu ion. This behavior of the doping dependence of $T_C(x)$ is in good qualitative agreement with the experimental data [8–12].

It must be noted that for example, in Mn- or Cr-doped CAO on the Al site, where the ionic radius of Mn^{3+}(0.72 $\dot{A}$) or Cr^{3+}(0.63 $\dot{A}$) is larger than that of Al^{3+}(0.51 $\dot{A}$), the lattice parameters increase in agreement with the experimental data of Zhang et al. [15]. A tensile strain appears, i.e., J_d decreases, which leads to a decrease in M_s with increasing Mn or Cr ion doping concentration (see Figures 3 and 4, respectively). Similar behavior is reported for Cu(Al,Mn)O_2 by Zhang et al. [15]. Unfortunately, there are not experimental data for $M(x)$ of Cr-doped CAO. A decrease in the magnetization is observed additively with increasing Mn content x due to the antiferromagnetic coupling among the Mn spins (contrary to the case of Mn doping at the Cu site). By the substitution of the Al ion with a rare earth ion (RE) whose radius is larger than that of Al, tensile strain and a reduction of the spontaneous magnetization M_s with an increase in the RE ion doping concentration appears again. Unfortunately, there are not experimental data for RE doped CAO.

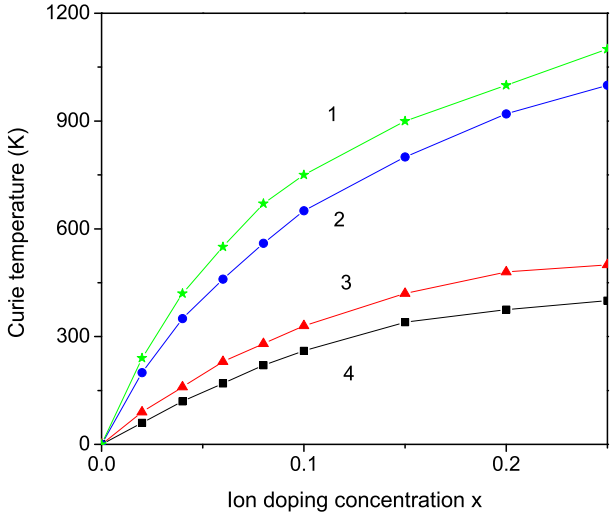

Figure 2. (Color online) The Curie temperature T_C as a function of the ion doping concentration x for different ions substituted the Cu ion: (1) Fe; (2) Co; (3) Mn; and (4) Ni.

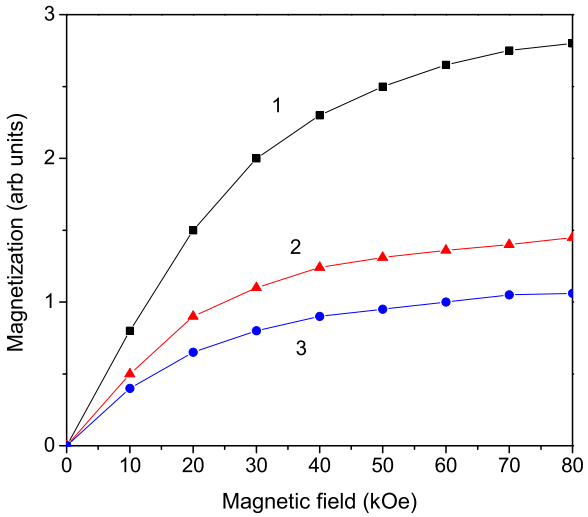

Figure 3. (Color online) Magnetic field dependence of the magnetization M_s of Cu(Al,Mn)O_2 for different Mn-ion doping concentrations x: (1) 0.01; (2) 0.03; and (3) 0.05.

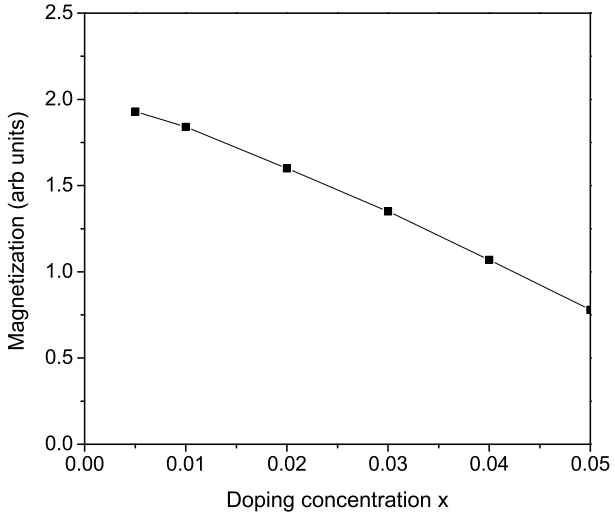

Figure 4. Dependence of the magnetization M_s of Cu(Al,Cr)O_2 on the doping Cr ion concentration.

From Equation (8), we have calculated the band-gap energy E_g for pure and ion-doped CAO NPs (see Figure 5). It must be noted that there is a broadening of the band gap E_g of pure CAO NPs with a decrease in the NP size. We now consider the case of a Cr^{3+}-doped CAO NP, $CuAl_{1-x}Cr_xO_2$. The lattice parameters increase with the increase in the Cr-doping concentration [17] because the ionic radius of the doping Cr ion (0.63 $\dot{A}$) is larger than that of the host Al ion (0.51 $\dot{A}$). A tensile strain appears, i.e., J_d decreases with increasing x, which leads to a decrease in the magnetization (see Figure 4) and an increase in E_g (curve 1). The observed behavior is in agreement with the experimental data of Jiang et al. [17]. We would also obtain a similar enhanced E_g within our model by doping with Sb^{3+} (0.76 $\dot{A}$) ions or Y^{3+} (1.04 $\dot{A}$) ions, which also causes a tensile strain, i.e., an increase in the lattice parameters as well as a decrease in the exchange interaction constant J_d and therefore reduced magnetization M_s and enhanced E_g, reported in [18,31]. Otherwise, by doping with the Mg ion, we observe the contrary result: a decrease in the band-gap energy (curve 2), in agreement with [28,30,32]. The optical absorption of the CAO increases due to the reduction in E_g by Mg doping. A smaller E_g is also reported by Bi and Eu doping at the Al site in CAO [21,33].

Finally, we will discuss the temperature, size, and ion-doping dependence of the phonon energy ω and damping γ in CAO NPs. The temperature dependence for the A_{1g} mode ω_0 = 767 cm^{-1} of the phonon energy ω and phonon damping γ is shown in Figure 6. We take into account the anharmonic spin–phonon interaction $R < 0$, as well as the three-phonon $A > 0$ and four-phonon $B < 0$ anharmonic interactions. Let us emphasize that in order to obtain the experimentally observed softening of ω, we have to chose $R < 0$. For $R > 0$, we would obtain a hardening, an increase in ω with T [34]. The damping γ is proportional to R^2 and so independent of the sign of R. γ corresponds to the full width at half-maximum of the Raman lines and is indirectly proportional to the phonon life time. The damping is a direct consequence of the anharmonic coupling. The phonon energy decreases, whereas the phonon damping increases with increasing temperature, which is in agreement with [22,26]. It can be seen from Figure 6 that around $T_c \sim 400$ K, we observe a kink due to the spin–phonon interaction R. For $R = 0$, the kink disappears. Moreover, the kink is size-dependent; it shifts to smaller T values with increasing NP size. In Figure 1, we have shown that with decreasing NP size spontaneous magnetization M_s with the corresponding T_C value appears. A similar anomaly in the phonon energy and damping of CAO thin films is observed experimentally between 423 and 573 K by Singh et al. [22] and around $T \sim 300$ K by Pellicer-Porres et al. [26]. The authors have proposed that these changes may be related to a negative thermal expansion (NTE) in the delafossite structure

along the O-Cu-O linkage. A similar NTE is also reported in other AMO_2 (A = Cu or Ag; M = Al, Sc, In, or La) [35–37]. NTE means a volume contraction, i.e., there is a change in the structure, for example, by transitions between ferro- and paramagnetic phases.

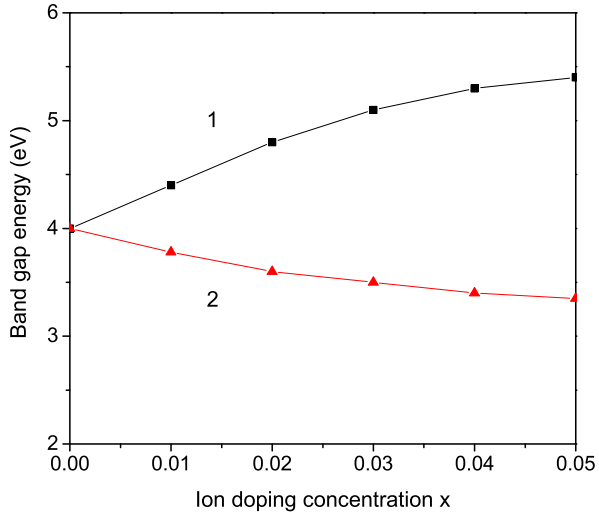

Figure 5. (Color online) Dependence of the band-gap energy E_g on the doping concentration x for a Cr-doped (1) and Mg-doped (2) substitution of the Al ion in CAO NP, N = 10, and T = 300 K.

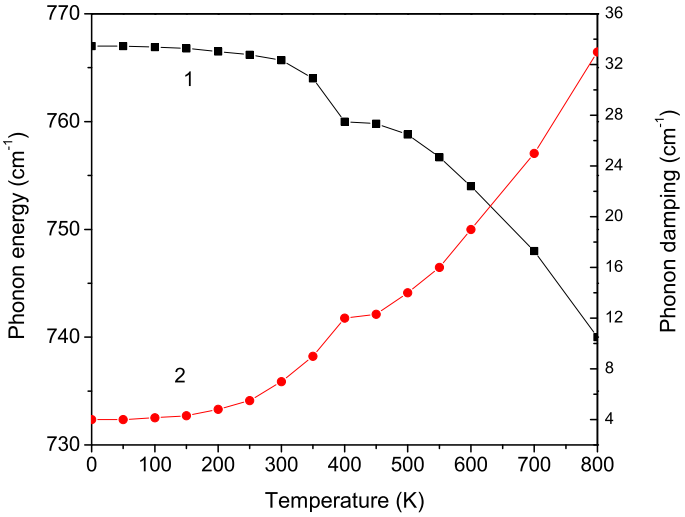

Figure 6. (Color online) Temperature dependence of the phonon energy ω (1) and phonon damping γ (2) of a CAO NP, N = 10.

The size dependence of the phonon energy ω and the phonon damping γ in a CAO NP is presented in Figure 7. It can be seen that the phonon energy decreases whereas the damping increases with decreasing nanoparticle size, which is in agreement with the experimental data of Yassin et al. [23].

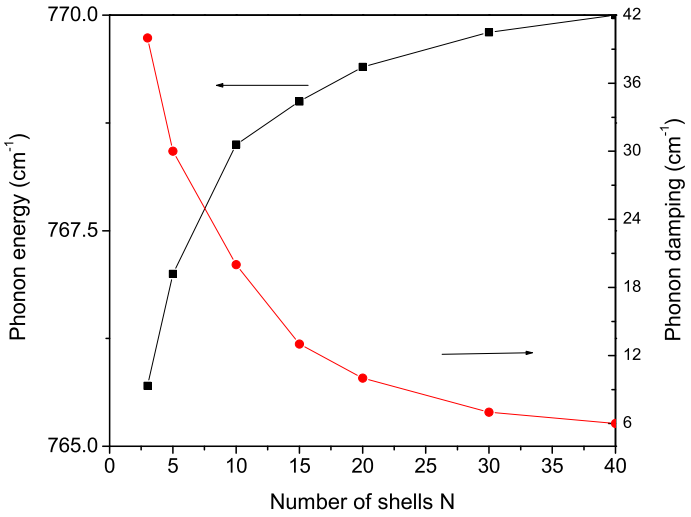

Figure 7. (Color online) Size dependence of the phonon energy ω and phonon damping γ of a CAO NP, T = 300 K.

The ion-doping also influences the phonon properties of CAO NPs. It may cause lattice distortions and unrelaxed strains. To show this, we will consider the Fe^{3+} doping at the Al^{3+} site. The ionic radius of the Fe ion (0.65 $\dot{A}$) is larger than that of the Al ion (0.51 $\dot{A}$), i.e., we observe tensile strain, an increase in the lattice parameters that leads to a decrease in J_d and R_d and to a decrease in the phonon energy with increasing Fe ions, see Figure 8, curve 1. This corresponds to a red-shift in the peak positions. The contribution to the damping of the ion doping is in addition to those of the bulk, surface, spin–phonon, and phonon–phonon interactions, so that γ increases with increasing Fe concentration (see Figure 8, curve 2). This means that the full-weight of the half maximum increases, i.e., the Raman lines are broadener. This is in agreement with the experimental results of Fe-doped CAO [38]. We obtain a similar decrease in ω and an increase in γ for Eu-doped CAO NP as reported by Liu et al. [21].

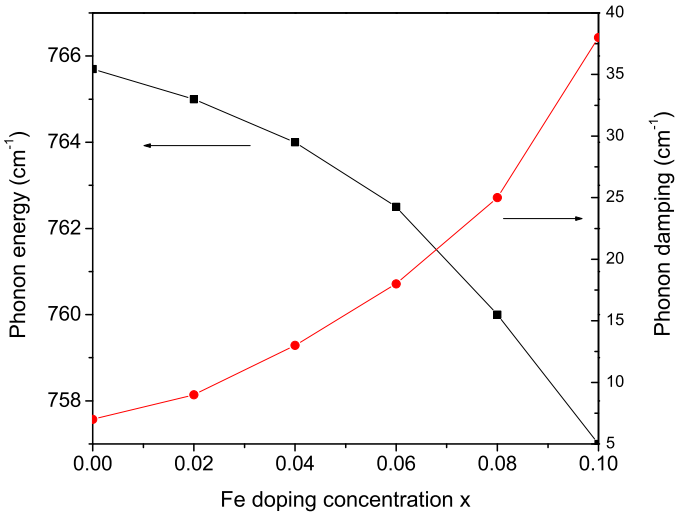

Figure 8. (Color online) Fe ion-doping dependence of the phonon energy ω and phonon damping γ of a $Cu(Fe,Al)O_2$ NP, N = 10, and T = 300 K.

4. Conclusions

To conclude, we have studied the size and ion-doping effects on the magnetic, optical, and phonon properties of transition metal (TM = Fe, Co, Mn, and Ni) ion-doped CAO NPs on the Cu and Al site using a microscopic model and Green's function theory. The RTFM in bulk CAO can be due to ion doping, whereas CAO NPs make an additive contribution in terms of surface and size effects . Due to surface defects, a magnetization is obtained that increases with decreasing NP size. The difference in the radii of the TM^{3+} and the host Cu^{+} ions leads to a compressive strain, an increase in the exchange interaction constants, and increased spontaneous magnetization M_s and Curie temperature T_C. The doping TM^{3+} ion has an additional spin value compared to the zero spin value of the Cu^{+} ion, which also enhances M_s. On the other hand, a tensile strain is observed by substitution with Mn^{3+} or Cr^{3+} on the Al^{3+} site, where the radius of the Mn or Cr ions is larger than that of the Al ion, which leads to a decrease in M_s with an increase in the ion-doping concentration. The band-gap energy increases with decreasing NP size and by doping with Cr or Sb ions and decreases by Mg ion doping. The phonon energy ω decreases, whereas the phonon damping γ increases, with increasing temperature. They show a kink around the phase-transition temperature $T_C \sim 400$ K, caused by the anharmonic spin–phonon interaction. Due to surface and size effects, ω decreases, whereas γ increases, with decreasing NP size. The phonon energy decreases, whereas the damping increases, by Fe and Eu doping on the Al site, i.e., a red shift and broadening of the Raman peaks is obtained. The observed results are in good qualitative agreement with the existing experimental data.

Let us emphasize that in order to take into account the carrier doping treatment in transition-metal-doped CAO on the Cu site, which plays an additive role in the effect of the different ionic radii, we have to expand our model and consider the s-d model by also taking into account the electron–phonon interaction, which is important for CAO [39]. This could be done in the next paper.

Author Contributions: All authors contributed equally to this work. All authors have read and agreed to the published version of the manuscript.

Funding: This research received no external funding.

Data Availability Statement: The raw data that support the findings of this study are available from the corresponding author upon reasonable request.

Conflicts of Interest: The authors declare no conflict of interest.

References

1. Dietl, T.; Ohno, H.; Matsukura, F.; Cibert J.; Ferrand, D. Zener Model Description of Ferromagnetism in Zinc-Blende Magnetic Semiconductors. *Science* **2000**, *287*, 1019. [CrossRef]
2. Sato, K.; Dederichs, P.H.; Katayama-Yoshida, H. Curie temperatures of III-V diluted magnetic semiconductors calculated from first principles. *Europhys. Lett.* **2003**, *61*, 403. [CrossRef]
3. Sato K.; Katayama-Yoshida, H. First principles materials design for semiconductor spintronics. *Semicond. Sci. Technol.* **2002**. *17*, 367. [CrossRef]
4. Kizaki, H.; Sato K.; Katayama-Yoshida, H. Materials Design of $CuAlO_2$-Based Dilute Magnetic Semiconductors by First-Principles Calculations and Monte Carlo Simulations. *Jpn. J. Appl. Phys.* **2008**, *47*, 6488. [CrossRef]
5. Iordanidou K.; Persson, C. Stoner Ferromagnetism in Hole-Doped $CuM^{IIIA}O_2$ with M^{IIIA} = Al, Ga, and In. *ACS Appl. Mater. Interfaces* **2021**, *13*, 29770. [CrossRef]
6. Kawazoe, H.; Yasukawa, M.; Hyodo, H.; Kurita, M.; Yanagi H.; Hosono, H. P-Type Electrical Conduction in Transparent Thin Films of $CuAlO_2$. *Nature* **1997**, *389*, 939. [CrossRef]
7. Kizaki, H.; Sato, K.; Katayama-Yoshida, H. Carrier concentration dependence of Curie temperature in $CuAlO_2$ based dilute magnetic semiconductor by first-principles calculations. *Phys. Stat. Sol. (c)* **2007**, *3*, 4135. [CrossRef]
8. Aziziha, M.; Byard, S.A.; Beesely, R.; Lewis, J.P.; Seehra, M.S.; Johnson, M.B. Magnetic properties of Fe-doped $CuAlO_2$ and role of impurities. *AIP Adv.* **2019**, *9*, 035030. [CrossRef]
9. Chen, C.; Dong, C.; Wang, B.; Huang, J.; Wang, Y. Synthesis and Room Temperature Ferromagnetism in Fe-Doped $CuAlO_2$ Semiconductor. *J. Wuhan Univ. Technol.-Mater. Sci. Ed.* **2013**, *28*, 500. [CrossRef]
10. Dong, C.J.; Yu, W.X.; Xu, M.; Cao, J.J.; Zhang, Y.; Chuai, Y.H.; Wang, Y.D. Evidence of room temperature ferromagnetism in Co-doped transparent $CuAlO_2$ semiconductor. *J. Alloys Compd.* **2012**, *512*, 195. [CrossRef]

11. Wang, Y.; Dong, C.; Chuai, Y.; Wang, Y. Room temperature ferromagnetism in Codoped $CuAlO_2$ nanofibers fabricated by electrospinning. *J. Wuhan Univ. Technol.-Mater. Sci.* **2015**, *30*, 1. [CrossRef]
12. Ray, N.; Gupta, V.; Sarma, L.; Kush, P.; Nag, J.; Sapra, S. Tuning the Electronic and Magnetic Properties of $CuAlO_2$ Nanocrystals Using Magnetic Dopants. *ACS Omega* **2018**, *3*, 509. [CrossRef]
13. Hidetoshi, K.; Kazunori, S.; Akira, Y.; Katayama-Yoshida, H. First-Principles Materials Design of $CuAlO_2$ Based Dilute Magnetic Semiconducting Oxide. *Jpn. J. Appl. Phys.* **2005**, *44*, L1187.
14. Sun, C.Q. Dominance of broken bonds and nonbonding electrons at the nanoscale. *Nanoscale* **2010**, *2*, 1930. [CrossRef] [PubMed]
15. Zhang, H.Y.; Li, P.G.; Chen, C.P.; Tu, Q.Y.; Tang, W.H. Magnetic properties of Mn-doped transparent $CuAlO_2$ semiconductor. *J. Alloys Compd.* **2005**, *396*, 40.
16. Lalic, M.V.; Mestnik-Filho, J.; Carbonari, A.W.; Saxena, R.N.; Moralles, M. Influence of Cd impurity on the electronic properties of $CuAlO_2$ delafossite: First-principles calculations. *J. Phys. Condens. Matter* **2002**, *14*, 5517. [CrossRef]
17. Jiang, H.F.; Zhu, X.B.; Lei, H.C.; Li, G.; Yang, Z.R.; Song, W.H.; Dai, J.M.; Sun,Y.P.; Fu, Y.K. Effect of Cr doping on the optical-electrical property of $CuAlO_2$ thin films derived by chemical solution deposition. *Thin Solid Films* **2011**, *519*, 2559.
18. Liu, Y.; Huang, Y.; Seo, H.J.; Wu, Y. Blueshift in near-band-edge emission in Y^{3+}-doped $CuAlO_2$ nanofibers. *Opt. Mater. Express* **2014**, *4*, 2602. [CrossRef]
19. Liu, R.; Li, Y.; Yao, B.; Ding, Z.; Jiang, Y.; Meng, L.; Deng, R.; Zhang, L.; Zhang, Z.; Zhao, H.; et al. Shallow Acceptor State in Mg-Doped $CuAlO_2$ and Its Effect on Electrical and Optical Properties: An Experimental and First-Principles Study. *ACS Appl. Mater. Interfaces* **2017**, *9*, 12608. [CrossRef]
20. Zhao, X.; Zhang, M.; Bai, P.; Hou, X.; Liu, F.; Yan, H. Optical, electrical, and structural properties of Fe-doped $CuAlO_2$ thin films. *Funct. Mater. Lett.* **2019**, *12*, 1850106. [CrossRef]
21. Liu, Y.; Gong, Y.; Mellott, N.P.; Wang, L.; Ye, H.; Wu, Y. Luminescence of delafossitetype $CuAlO_2$ fibers with Eu substitution for Al cations. *Sci. Technol. Adv. Mater.* **2016**, *17*, 200. [CrossRef] [PubMed]
22. Singh, M.K.; Dussan, S.; Sharma, G.L.; Katiyar, R.S. Raman scattering measurements of phonon anharmonicity in thin films. *J. Appl. Phys.* **2008**, *104*, 113503. [CrossRef]
23. Yassin, O.A.; Alamri, S.N.; Joraid, A.A. Effect of particle size and laser power on the Raman spectra of $CuAlO_2$ delafossite nanoparticles. *J. Phys. D Appl. Phys.* **2013**, *46*, 235301. [CrossRef]
24. Benreguia, N.; Barnabe, A.; Trari, M. Sol–gel synthesis and characterization of the delafossite $CuAlO_2$. *J. Sol-Gel Sci. Technol.* **2015**, *75*, 670. [CrossRef]
25. Byrne, D.; Cowley, A.; Bennettc, N.; McGlynn, E. The luminescent properties of $CuAlO_2$. *J. Mater. Chem. C* **2014**, *2*, 7859. [CrossRef]
26. Pellicer-Porres, J.; Martinez-Garcia, D.; Segura, A.; Rodriguez-Hernandez, P.; Munoz, A.; Chervin, J.C.; Garro, N.; Kim, D. Pressure and temperature dependence of the lattice dynamics of $CuAlO_2$ investigated by Raman scattering experiments and *ab initio* calculations. *Phys. Rev. B* **2006**, *74*, 184301. [CrossRef]
27. Wesselinowa, J.M.; Apostolov, A.T. Self-consistent theory of spin–phonon interactions in ferromagnetic semiconductors. *J. Phys. Condens. Matter* **1993**, *5*, 3555. [CrossRef]
28. Agrawal, S.; Parveen, A.; Azam, A. Influence of Mg on structural, electrical and magnetic properties of $CuAlO_2$ nanoparticles. *Mater. Lett.* **2016**, *168*, 125. [CrossRef]
29. Luo J.; Lin, Y.-J. Point defect-induced magnetic properties in $CuAlO_2$ films without magnetic impurities. *Appl. Phys. A* **2016**, *122*, 163. [CrossRef]
30. Dong, G.; Zhang, M.; Lan, W.; Dong, P.; Yan, H. Structural and physical properties of Mg-doped $CuAlO_2$ thin films. *Vacuum* **2008**, *82*, 1321. [CrossRef]
31. Ghosh, C.K.; Popuri, S.R.; Sarkar, D.; Chattopadhyay, K.K. Sb-doped $CuAlO_2$: Widening of band gap and nonlinear J-E characteristics. *J. Mater. Sci.* **2011**, *46*, 1613. [CrossRef]
32. Zou, Y.S.; Wang, H.P.; Zhang, S.L.; Lou, D.; Dong, Y.H.; Song, X.F.; Zeng, H.B. Structural, electrical and optical properties of Mg-doped $CuAlO_2$ films by pulsed laser deposition. *RSC Adv.* **2014**, *4*, 41294. [CrossRef]
33. Daichakomphu, N.; Klongratog, B.; Rodpun, P.; Pluengphon, P.; Harnwunggmoung, A.; Poo-arporn, Y.; Sakulkalavek, A.; Sakdanuphab, R. Improving the photo-thermoelectric performance of $CuAlO_2$ *via* doping with Bi. *Mater. Res. Bull.* **2021**, *144*, 111479. [CrossRef]
34. Wesselinowa, J.M.; Apostolov, A.T. Anharmonic effects in ferromagnetic semiconductors. *J. Phys. Condens. Matter* **1996**, *8*, 473. [CrossRef]
35. Li, J.; Sleight, A.; Jones, C.Y.; Toby, B. Trends in negative thermal expansion behavior for AMO_2 (A=Cu or Ag; M=Al, Sc, In, or La) compounds with the delafossite structure. *J. Solid State Chem.* **2005**, *178*, 285. [CrossRef]
36. Miller, W.; Smith, C.W.; Mackenzie, D.S.; Evans, K.E. Negative Thermal Expansion: A Review. *J. Mater. Sci.* **2009**, *44*, 5441. [CrossRef]

37. Salke, N.P.; Rao, R.; Achary, S.N.; Tyagi, A.K. Raman spectroscopic investigations on delafossite $CuLaO_2$ at high pressures. *J. Phys. Conf. Ser.* **2012**, *377*, 012020. [CrossRef]
38. Aziziha, M.; Akbarshahi, S.; Ghosh, S.; Pramanik, P.; Lewis, J.P.; Romero, A.H.; Thota, S.; Seehra, M.S.; Johnson, M.B. Phonon Dynamics in Anisotropic Dilute $CuAl_{1-x}Fe_xO_2$ Delafossite Alloys by a Weighted Dynamical Matrix Approach. *J. Phys. Chem. C* **2019**, *123*, 30604. [CrossRef]
39. Nakanishi, A.; Katayama-Yoshida, H. Chemical trend of superconducting transition temperature in hole-doped delafossite of $CuAlO_2$, $AgAlO_2$ and $AuAlO_2$. *Solid State Commun.* **2012**, *152*, 2078. [CrossRef]